Published in final edited form as:
Nat Cell Biol. 2013 August ; 15(8): 937–947. doi:10.1038/ncb2802.

Vesicles modulate an actin network for asymmetric spindle positioning

Zuzana Holubcová, **Gillian Howard**, and **Melina Schuh**
Medical Research Council, Laboratory of Molecular Biology, Cambridge CB2 0QH, United Kingdom

Abstract

Actin networks drive many essential cellular processes, including cell migration, cytokinesis and tissue morphogenesis. But how cells organize and regulate dynamic actin networks that consist of long, unbranched actin filaments is only poorly understood. This study in mouse oocytes reveals that cells can use vesicles as adaptable, motorized network nodes to regulate the dynamics and density of intracellular actin networks. In particular, Rab11a-positive vesicles drive the network dynamics in a myosin-Vb-dependent manner, and modulate the network density by sequestering and clustering the network's actin nucleators. We also report a simple way by which networks of different densities can be generated, namely by adjusting the number and volume of vesicles in the cell. This vesicle-based mechanism of actin network modulation is essential for asymmetric positioning of the meiotic spindle in mouse oocytes, a vital step in the development of a fertilizable egg in mammals.

Dynamic actin networks have many essential functions in cells: they are required for cell migration[1,2], cytoplasmic organization[3], ingression of the cytokinetic furrow[4,5], cortical flows[6,7] and tissue morphogenesis[8,9]. Many actin networks consist of long, unbranched actin filaments, such as those that are nucleated by formins. However, little is known about how these linear filaments are reorganized into dynamic networks and how the dynamics and the density of these networks are controlled. More is known about Arp2/3-dependent actin networks. Here, network assembly depends on Arp2/3-dependent branching of actin filaments from the side of existing filaments. Arp2/3 nucleated networks are very dense and show relatively low contractility because they consist of crosslinked filaments[6,10]. Thus, network reorganization requires unbranching and filament severing[2,11,12]. We and others reported that mouse oocytes are filled with a highly dynamic actin network, which is nucleated by cooperation between two types of actin nucleators that assemble linear actin filaments: the formin Fmn2 and the recently discovered actin nucleators Spire1 and Spire2[13-16]. We reported recently that this actin network mediates long-range transport of vesicles[17]. In particular, we found that vesicles that are positive for the small GTPase Rab11a, which determines the vesicles' identity and function by recruiting vesicle-specific effector proteins[18], move over distances of up to 30 μm along actin filaments towards the oocyte surface[17]. This was surprising given that long-range vesicle transport is generally thought to occur along microtubules in animal cells, whereas transport along actin filaments is thought to be most relevant over short distances in specialized subcellular compartments such as dendritic spines and the actin cortex[19,20].

Correspondence: mschuh@mrc-lmb.cam.ac.uk; Tel: +44 (0)1223 267029; Fax: +44 (0)1223 268300.
Contributions: G.H. analysed the localisation of Spire2 by electron microscopy. Z.H. and M.S. designed and carried out all other experiments. M.S. and Z.H. wrote and edited the manuscript, respectively.

Competing financial interests: The authors declare no competing financial interests.

Europe PMC Funders Author Manuscripts

In this study, we set out to investigate the function of the Rab11a-positive vesicles that are transported by this actin-dependent mechanism in mouse oocytes. Unexpectedly, we found that these vesicles function as cytoskeletal modulators. The vesicles drive the dynamics of the actin network by recruiting myosin Vb to reorganize actin filaments, and regulate the network density by sequestering and clustering the nucleators of the network. The dynamic actin networks that are generated by this vesicle-dependent mechanism are robust, adaptable and rapidly restore a dynamic steady-state after reversal of perturbation. We also show that Rab11a-positive vesicles, myosin Vb and the vesicle-dependent dynamics of the actin network are required for asymmetric spindle positioning during oocyte maturation, an essential step in the development of a fertilisable egg in mammals. Based on our data, we suggest a model in which the movement of the spindle to the oocyte's surface is driven by the outward-directed dynamics of the vesicles and their associated actin filaments.

RESULTS

Asymmetric spindle positioning in oocytes requires Rab11a-positive vesicles

To investigate the function of the Rab11a-positive vesicles, we expressed a dominant-negative variant of Rab11a, Rab11a S25N. This led to the loss of Rab11a-positive vesicles from oocytes (Fig. 1a,b), which we confirmed by analysing the localization of the vesicles' cargo transferrin (Supplementary Fig. S1). We then analysed how the loss of Rab11a-positive vesicles affected oocyte maturation, the process by which an oocyte matures into a fertilizable egg. In the first step of maturation, the nucleus breaks down and a spindle assembles in the centre of the oocyte. The spindle is then asymmetrically positioned, which is a prerequisite for the asymmetric meiotic division that ensures that the egg contains sufficient storage material for embryo development and is crucial for fertility[21]. At the oocyte surface, the spindle segregates the homologous chromosomes and extrudes half of them in a very small cell termed the polar body. The other half of the chromosomes remains in the large egg, which is now ready for fertilisation. Depletion of Rab11a-positive vesicles neither affected the morphology (Supplementary Fig. S2a and Fig. 1c) nor the polarization of the oocytes, as indicated by the formation of an actin-rich and cortical granule free domain at the cortex in proximity of the spindle (Supplementary Fig. S2b,c). Likewise, the fraction of oocytes that underwent nuclear envelope breakdown, spindle assembly and anaphase, as well as the timing of meiotic progression were not significantly different (Supplementary Fig. S2d-h). Instead, we found that depletion of Rab11a-positive vesicles prevented asymmetric spindle positioning (Fig. 1c,f). To quantify this defect, we recorded three-dimensional (3D) data sets of spindle movement and tracked the spindle automatically in 3D. This confirmed that the spindle was static in dominant-negative Rab11a expressing oocytes (Fig. 1d,e). This defect was specifically due to the depletion of Rab11a-positive vesicles, because dominant-negative variants of other Rab-GTPases, such as Rab5a or Rab27a did not affect asymmetric spindle positioning (Fig. 1c-f).

The dynamics of an actin network depend on Rab11a-positive vesicles

We next analysed the reason why asymmetric spindle positioning failed when Rab11a-positive vesicles were depleted. We and others reported previously that asymmetric spindle positioning requires the oocyte's cytoplasmic actin network[13,14,16]. Thus, we tested whether asymmetric spindle positioning might fail because the actin network was affected. We reported recently that the vesicles localize to nodes in the actin network (Fig. 2a and Supplementary Video 1), that they recruit the nucleators of the network and that they serve as sites of actin nucleation[17]. Thus, we reasoned that the vesicles might be required to assemble the cytoplasmic actin network. However, oocytes were still filled with a network of intersecting actin filaments when Rab11a-positive vesicles were depleted (Fig. 2b and Supplementary Video 1). Only the prominent nodes of the actin network, which correspond

to the position of the vesicles, were missing. This suggests that the nucleators of the actin network are still active if Rab11a-positive vesicles are absent. Unexpectedly though, the actin network, which is normally very dynamic, was static when Rab11a-positive vesicles were lost (Fig. 2b and Supplementary Video 1). To quantify this defect, we recorded high resolution time-series of the network dynamics in control and dominant-negative Rab11a expressing oocytes (Supplementary Video 1) and performed an image correlation analysis (for details see methods). This confirmed that the dynamics of the actin network were severely impaired when the function of Rab11a-positive vesicles was blocked (Fig. 2c and Supplementary Fig. S3a). This result was surprising because it reveals that the actin network dynamics depend on Rab11a-positive vesicles.

The dynamics of the vesicles and their associated actin filaments drive asymmetric spindle positioning

Next, we investigated why asymmetric spindle positioning failed when the vesicle-dependent network dynamics were blocked. We reported previously that the spindle poles locally contract the network's actin filaments in a myosin light chain kinase-dependent manner and thereby pull on the network[16]. However, the mechanism by which the local pulling might mediate directional spindle movement remained unclear. Our recent work suggests that the Rab11a-positive vesicles and the actin filaments that are nucleated from their surface continuously move towards the plasma membrane[17]. Thus, an attractive hypothesis is that the pulling from the spindle poles couples the spindle to the outward-directed movement of the vesicles and their associated actin filaments. In this way, the spindle could move to the plasma membrane similarly to how vesicles move to the plasma membrane. The movement of the spindle to the cell surface could also involve direct temporary associations of vesicles with the spindle, which we observed throughout the entire process of asymmetric spindle positioning (Supplementary Video 2). Weak coupling and higher drag forces could explain why the spindle moves more slowly than the vesicles. To investigate whether the outward-directed dynamics of the vesicles and their associated actin filaments drive asymmetric spindle positioning, we first compared the interaction of the spindle with the vesicle-actin network in control oocytes and in oocytes that expressed dominant-negative Rab11a. While the spindle interacted dynamically with the vesicle-actin network in control oocytes, the spindle was immobile and trapped in the static actin network when Rab11a-positive vesicles were lost (Fig. 2d, Supplementary Fig. S3b, Supplementary Video 3 and 4). The spindle and the actin network were so static that we could even generate a high-resolution 3D reconstruction of the trapped spindle within the actin network from live oocytes (Supplementary Video 5). To test directly whether the dynamics of the vesicles and their associated actin filaments were required for asymmetric spindle positioning, we analysed whether we could artificially trap the spindle by blocking the network dynamics. For this purpose, we stabilized the vesicle-actin network by overexpressing very high amounts of the actin binding domain of Utrophin (Fig. 3a). This did indeed efficiently block asymmetric spindle positioning (Fig. 3b-e). Consistent with this result, the actin stabilizing drug jasplakinolide also blocked asymmetric spindle positioning (Supplementary Fig. S4). Together, these data are consistent with a model in which the outward-directed vesicle and actin filament dynamics drive asymmetric spindle positioning (Figure 8).

Myosin Vb mediates the actin network dynamics and asymmetric spindle positioning

We then investigated the mechanism that would explain the requirement of vesicles for the dynamics of the actin network. We reasoned that the vesicles must recruit a force generator that mediates the network dynamics by reorganizing filaments of the network. Myosin II has long been implicated in rearranging actin filaments[6], and recent *in vitro* data demonstrated that other myosins can also drive the re-organization of actin networks[12]. We reported recently that Rab11a-positive vesicles recruit myosin Vb in mouse oocytes[17]. To test

whether the actin network dynamics were myosin-Vb-dependent, we blocked myosin Vb function by expressing a dominant-negative tail construct. Dominant-negative myosin Vb blocked the network dynamics (Fig. 4a and Supplementary Video 6), as quantitatively confirmed by image correlation analysis (Fig. 4b and Supplementary Fig. S5).

Consistent with the model that asymmetric spindle positioning requires the outward-directed vesicle and actin filament dynamics, dominant-negative myosin Vb also blocked asymmetric spindle positioning (Fig. 4c-f). This defect was specifically due to blocking the function of myosin Vb because dominant-negative constructs of related myosins did not affect asymmetric spindle positioning (Fig. 4c-f). Consistent with this result, depletion of myosin Vb by RNAi also blocked asymmetric spindle positioning (Supplementary Fig. S5b-e).

Rab11a-positive vesicles modulate the actin network density

To investigate whether the vesicles also modulated other properties of the actin network in addition to its dynamics, we quantified the actin network density in control oocytes and in oocytes expressing dominant-negative Rab11a. In support of the model that the vesicles act as network modulators, the network density was significantly increased in dominant-negative Rab11a expressing oocytes (Fig. 5a,b). This increase was specifically due to the loss of Rab11a-positive vesicles, because dominant-negative variants of other Rab GTPases did not affect the network density (Fig. 5a,b). Next, we investigated whether a denser network is automatically less dynamic. To this end, we increased the network density to the same degree that we observed upon dominant-negative Rab11a expression by moderately overexpressing the network nucleators Fmn2 and Spire2 (Supplementary Fig. S6a,b). Our quantitative network dynamics assay revealed that the network was still dynamic (Supplementary Fig. S6c,d). Also the dynamics of asymmetric spindle positioning were not affected (Supplementary Fig. S6e-h), suggesting that the block of asymmetric spindle positioning in dominant-negative Rab11a expressing oocytes is not due to the ~2-fold increase in actin network density, but caused by the absence of the outward-directed dynamics of the vesicles and their associated actin filaments.

Although the increased network density in dominant-negative Rab11a expressing oocytes was not directly relevant for asymmetric spindle positioning, it still seemed important to investigate the mechanism by which the vesicles modulated the actin network density to improve our understanding of how dynamic actin networks of different densities can be generated. As reported above, we found recently that the nucleators of the actin network localize to the Rab11a-positive vesicles, from where actin filaments were nucleated[17]. We reasoned that recruitment of the nucleators to Rab11a-positive vesicles might help to modulate the precise topology and meshsize of the network. If the nucleators are sequestered and clustered on vesicles, the network density should be decreased (Fig. 5l). The Rab11a-positive vesicles do indeed seem suitable for sequestering and clustering the nucleators: their membrane surface is likely to be highly increased because Rab11a, the nucleators of the actin network, the membrane probe FM 1-43 and transferrin were found throughout the entire vesicle by light or electron microscopy (Fig. 5c-g and Supplementary Fig. S7a). This is unlikely to represent localization to the lumen, but might reflect that the membrane of the Rab11a-positive vesicles is highly folded or that the large Rab11a-positive vesicles that we observe consist of aggregates of smaller Rab11a-positive vesicles. Since only the fraction of actin nucleator on the periphery of the vesicle is in direct contact with the cytoplasm and thus able to contribute to network formation, the Rab11a-positive vesicles could effectively limit the amount of nucleator that can participate in network assembly. Expression of dominant-negative Rab11a would release the nucleators from the vesicles and could explain the increase in network density that we observed (Fig. 5l).

To test whether the vesicles modulate the network density by sequestering and clustering the nucleators, we first examined how the loss of Rab11a-positive vesicles affected the distribution of the actin nucleators Spire1, Spire2 and Fmn2. We found that all nucleators were released from vesicles in dominant-negative Rab11a expressing oocytes (Fig. 5h and Supplementary Fig. S7b,c). To recruit overexpressed Fmn2 to Rab11a-positive vesicles, also Spire1 or Spire2 had to be overexpressed, which is consistent with previous studies[17,22]. To quantify the redistribution of the nucleators, we developed an assay that allowed us to acutely deplete Rab11a-positive vesicles from the cell. We reasoned that brefeldin A (BFA), a drug which has been reported to affect the formation of recycling vesicles in other cell types, might be suitable for this purpose[23-26]. Indeed, acute addition of BFA blocked the formation of Rab11a-positive vesicles and led to the stepwise loss of vesicles over a period of ~15-20 minutes due to their outward-directed movement (Fig. 5i,j and Supplementary Fig. S8 and Supplementary Video 7). In some oocytes, a few vesicles in the centre of the oocyte remained, which is consistent with our previous observation that vesicles in the oocyte's centre are less likely to move to the surface[17]. The loss of Rab11a-positive vesicles could also explain why asymmetric spindle positioning fails in BFA-treated oocytes[27]. We then analysed how vesicle depletion by BFA affected the distribution of the actin nucleators. Quantification of the cytoplasmic mEGFP-Spire2 intensity showed that the amount of nucleator in the cytoplasm increased as the number of vesicles decreased (Fig. 5i-k and Supplementary Video 7). Consistent with this result, also Spire1 and Formin-2 were released from vesicles in BFA treated cells (Supplementary Fig. S8b,c). Together, these data suggest that vesicles modulate the density of the actin network by sequestering and clustering the network's actin nucleators Spire1, Spire2 and Fmn2.

Actin networks of different densities can be generated by adjusting the number and volume of Rab11a-positive vesicles

Our model predicts that the assembly of a dense actin network should involve a high number of vesicles whereas a wide-meshed actin network should only involve a low number of vesicles (Fig. 5l). To test this prediction, we first quantified the number and volume of the Rab11a-positive vesicles (Fig. 6b-d) and measured the density of the actin network (Fig. 6e,f) in different stages of oocyte maturation (Fig. 6a). Before nuclear envelope breakdown, oocytes contained a very high number of small vesicles. Correspondingly, the actin network was very dense (Fig. 6b-f, Before NEBD). Around nuclear envelope breakdown, the number of vesicles dropped as small vesicles merged into larger vesicles. This was accompanied by a strong decrease in the network density (Fig. 6b-f, NEBD), which is consistent with a previous study[27]. The number of vesicles stayed low while the spindle assembled (3h after NEBD) and moved to the cell surface (6h after NEBD). Accordingly, the network density stayed low in these stages as well (Fig. 6b-f, 3h and 6h after NEBD). These data demonstrate that the actin network density correlates with the number of vesicles.

Next, we tested whether we could artificially modulate the network density by altering the number of vesicles. We reasoned that we should be able to generate a high number of small vesicles by first depleting Rab11a-positive vesicles from oocytes using BFA and by subsequently washing out BFA to trigger the simultaneous reformation of a high number of vesicles. To test this possibility, we quantified the number and volume of vesicles upon BFA washout. Indeed, we found that the oocytes contained a high number of small vesicles four minutes after BFA washout (Fig. 7a-c). Consistent with our model, the network density was significantly increased (Fig. 7a,d). Interestingly, we observed that the system quickly restored its original configuration after BFA washout. In a stepwise manner, the small vesicles merged into larger vesicles (Fig. 7a-c). The resulting decrease in the number of vesicles was accompanied by a stepwise decrease in actin network density (Fig. 7a,d). After about 18 minutes, the oocytes were not distinguishable from control oocytes anymore (Fig.

7a-d). Together, these data suggest that the actin network density can be modulated by altering the number of Rab11a-positive vesicles and that the dynamic actin networks that are generated by this vesicle-based mechanism are robust and rapidly restore a dynamic steady-state after reversal of perturbation. To investigate whether vesicle abundance and network density are also coupled when the network density is altered by the amount of nucleator in the oocyte[14,28], we highly co-overexpressed the nucleators Fmn2 and Spire2, which strongly increases the network density (Fig. 7e)[14]. Consistent with coupling, the increase in network density was accompanied by a large increase in the number of Rab11a-positive vesicles and a decrease in their volume (Fig. 7f-h). Together, these data are consistent with the model that the generation of actin networks of different densities involves an adjustment of the number of Rab11a-positive vesicles.

DISCUSSION

In conclusion, this study reveals an unexpected vesicle-based mechanism by which cells can generate dynamic actin networks of different densities. The vesicles drive the dynamics of the actin network in a myosin-Vb-dependent manner and modulate the network density by clustering and sequestering the nucleators of the network. In this way, the vesicles act as force generators as well as actin nucleating centres at the same time. The dynamic actin networks that are generated by this vesicle-based mechanism are robust, adaptable and rapidly restore a dynamic steady-state after reversal of perturbation.

Assembling dynamic actin networks by clustering nucleators of unbranched actin filaments and myosins on membranes in ‘actin organizing centres’ might represent a general principle of cytoskeletal organization. In fission yeast, the contractile ring is initially made up of a coarsely-meshed actin network that converges at plasma membrane-bound nodes[29]. Like Rab11a-positive vesicles in mouse oocytes, these membrane-bound nodes are enriched in a formin, a myosin and actin. During cytokinesis, these membrane-bound nodes merge with each other to form a contractile ring[5,29]. Based on these similarities, it is tempting to speculate that dynamic cortical actin networks can be organized from clusters of actin nucleators and myosins at the plasma membrane, whereas intracellular dynamic actin networks can be organized by clustering of actin nucleators and myosins on vesicles, as shown in this study. Indeed, morphologically similar actin networks that converge at bright actin nodes, which might correspond to membrane-associated ‘actin organizing centres’, have been reported in a range of cell types, including *Xenopus* epithelial cells[30], *Drosophila* embryos[9] and oocytes[31], and *C.elegans* embryos[7]; and actin nucleation has been observed on vesicles in *Xenopus* egg extracts[32,33] and zebrafish embryos[33].

In addition to revealing an elegant mechanism for organizing dynamic actin networks, this work also provides important insights into the mechanism of asymmetric spindle positioning in oocytes. Oocytes need to divide extremely asymmetrically to preserve sufficient storage material for the development of the embryo. In mammals, including humans, this requires that the spindle moves from the centre to the surface of the oocyte using a cytoplasmic actin network[13,16]. Our data reveal a vital function for Rab11a-positive vesicles in this process: if the function of the Rab11a or myosin-Vb is blocked the spindle is unable to move to the oocyte’s surface. Our data are consistent with a model in which myosin light chain kinase-dependent pulling from the spindle poles[16] and direct association of Rab11a-positive vesicles with the spindle couple the spindle to the outward moving vesicles and the actin filaments that are nucleated from their surface (Fig. 8).

Dynamic actin networks have many essential functions in cells. This study reveals a vesicle-based mechanism by which cells can generate dynamic actin networks of different densities. This function of vesicles as cytoskeletal modulators is essential for asymmetric positioning

of the meiotic spindle in oocytes. Since defects during asymmetric oocyte division result in pregnancy loss and infertility[21], this mechanism of vesicle-based actin network organization is not only of fundamental scientific interest but also vital for mammalian reproduction.

METHODS

Preparation and culture of oocytes

All mice were maintained in a specific pathogen-free environment according to UK Home Office regulations. Oocytes were isolated from ovaries of 8-week-old FVB mice, cultured, and microinjected as described in detail before[34]. Oocytes microinjected with mRNA encoding fluorescently labelled proteins were arrested in dbcAMP until protein was expressed. Oocytes were then released into dbcAMP free medium. In some experiments, oocytes were treated with 10 μM BFA (brefeldin A, Sigma), 50 nM jasplakinolide (Calbiochem), 5 μM FM 1-43 (Molecular Probes), Alexa Fluor 488-labelled transferrin (Molecular Probes) or Cy5-labelled transferrin (gift from B. Nichols, MRC LMB, Cambridge, UK). The live oocytes in Figure 2d were briefly treated with 0.05 μg/ml Hoechst 33342 (Molecular Probes) to label chromosomes. For depletion of myosin Vb by RNAi the following siRNAis from QUIAGEN were used: Mm_Myo5b_2 SI01322202 AACCTGGAGTTTCTCAATGAA, Mm_Myo5b_3 SI01322209 TCAAACTGAGATAATATTAAA, Mm_Myo5b_4 SI01322216 CCGGAAGGTG GATTTGTTAAA. 3.5 pl of 1.8 μM siRNAs were microinjected into follicle-enclosed oocytes from 10-12-day-old (C57BL × CBA) F1 females and then cultured for about 10 days by methods described before[14]. The oocytes in Supplementary Fig. S2b and S2c were isolated from follicles of (C57BL × CBA) F1 females that were grown *in vitro* as previously described[14], because they are more likely than oocytes from FVB females to form the spindle at an asymmetric position due to an initially asymmetric position of the nucleus.

Expression constructs and mRNA synthesis

To generate the constructs for *in vitro* mRNA synthesis, the previously published protein coding sequences were fused with mCherry[35] to obtain mCherry-Rab5a S34N[36], mCherry-Rab27a T23N[37] and mCherry-MAP4[34] and inserted into pGEMHE[38] for *in vitro* transcription. These constructs as well as pGEMHE-mEGFP-Rab11a[17], pGEMHE-mCherry-Rab11a[17], pGEMHE-mEGFP-Rab11a S25N[17], pGEMHE-mCherry-Rab11a S25N[17], pGEMHE-H2B-mRFP1[34], pGEMHE-EGFP-MAP4[34], pGEMHE-Spire2-mCherry[14], pGEMHE-Spire2-mEGFP[14], pGEMHE-Spire1-mEGFP[14] pGEMHE-mCherry-myosin Vb tail[17], pGEMHE-mCherry-myosin VI Tail[17] and pGEMHE-mCherry-myosin Va Tail[17] were linearised with AscI. Capped mRNA was synthesized using T7 polymerase (mMessage mMachine kit, following manufacturer's instructions, Ambion) and dissolved in 11 μl water. pCS2-Fmn2-mCherry[16] and pCS2-EGFP-UtrCH[39] were linearised with BssHII or NsiI respectively. Capped mRNAs were synthesized using SP6 polymerase (mMessage mMachine kit, Ambion), polyadenylated (Poly(A) Tailing Kit, Ambion) and dissolved in 6 μl water. mRNA concentrations were determined on ethidium bromide agarose gels by comparison with an RNA standard (Ambion).

Confocal microscopy

Images were acquired with a Zeiss LSM710 confocal microscope equipped with a Zeiss environmental incubator box or a Zeiss LSM780 confocal microscope equipped with a Tokai Hit Stage Top Incubator, with a 40× C-Apochromat 1.2 NA water immersion objective lens for live oocytes, and a 63× C-Apochromat 1.2 NA water immersion objective for fixed oocytes as previously described[34]. In some images, shot noise was reduced with a Gaussian filter.

Immunofluorescence

Oocytes were fixed for 30 min at 37°C in 100 mM HEPES (pH 7) (titrated with KOH), 50 mM EGTA (pH 7) (titrated with KOH), 10 mM MgSO4, 2% formaldehyde (MeOH free) and 0.2% Triton X-100, based on previously published methods. Oocytes were left in PBS, 0.1% Triton X-100 overnight at 4°C. F-actin was stained with Alexa Fluor 488 phalloidin (Molecular Probes; 0.33 μM / 10 units/ml). Cortical granules were stained with *Lens culinaris* agglutinin (LCA) coupled with FITC (Sigma, 20 μg/ml). DNA was stained with 0.05 μg/ml Hoechst 33342 (Molecular Probes). All stainings were performed in PBS, 0.1% Triton X-100, 3% BSA.

Electron microscopy

Oocytes were fixed in 3% paraformaldehyde plus 0.5% glutaraldehyde in 100 mM HEPES (pH 7) (titrated with KOH), 50 mM EGTA (pH 7) (titrated with KOH), 10 mM MgSO4 buffer for 3 hours at room temperature and then transferred to 1% paraformaldhyde overnight at 4°C. After several buffer washes in phosphate buffer pH 7.4, inactivation of reactive aldehyde groups using 50 mM glycine in phosphate buffer for 30 min, was followed by permeabilisation with 0.03% saponin in 20 mM phosphate buffer, 150 mM Sodium Chloride. Oocytes were then incubated in normal goat serum (Aurion) for 40 min prior to overnight incubation at 4°C in rabbit anti-GFP antibody (Abcam 6556) used at 1:800. After thorough washing, oocytes were incubated in a 1:200 dilution of goat anti rabbit ultrasmall gold (Aurion) overnight at 4°C. Oocytes were then fixed in 2% glutaraldehyde in phosphate buffer, washed with distilled water followed by silver enhancement of gold using R-Gent SE-EM (Aurion) reagents and post fixed with 0.5% Osmium Tetroxide in 0.1M Phosphate buffer on ice for 15 min, washed in distilled water and dehydrated in an ascending ethanol series and embedded in CY212 resin. Ultrathin sections were stained with saturated aqueous Uranyl Acetate and Reynolds Lead Citrate and examined using a Philips 208 EM operated at 80kV.

Measurement of the cytoplasmic actin network density

To quantify the density of the cytoplasmic actin network in oocytes, the mean intensity of the Alexa Fluor 488 phalloidin staining was measured in the cytoplasm and in a region outside of the oocyte for background subtraction. Images in control and perturbed situations were acquired with identical imaging conditions and care was taken that images were not saturated during acquisition. Average, standard deviation, and statistical significance based on Student's t-test were calculated in Excel.

Quantification of actin network dynamics

To quantify the dynamics of the cytoplasmic actin network we expressed UtrCH-EGFP to label F-actin and recorded high resolution time series of the actin network in live mouse oocytes around the time of asymmetric spindle positioning (time interval 1.57 s). Images in control and perturbed situations were acquired with identical imaging conditions and care was taken that images were not saturated during acquisition. We then correlated each image in the time series with the first time frame in ImageJ using the Image CorrelationJ plugin[40]. In particular, images were correlated by calculating mean intensities in a local region of five pixels. The average correlation coefficients for the entire image were then plotted against time (Supplementary Figures S3a and S5a). For Figures 2c and 4b, actin networks were considered as dynamic if the correlation coefficient after 30 s was below 0.5 and as static if the correlation coefficient after 30 s was higher than 0.5. Average, standard deviation, and statistical significance based on Student's t-test were calculated in Excel.

Automated 3D tracking of the spindle

To measure the kinetics of asymmetric spindle positioning, we injected oocytes with mRNA encoding fluorescently labelled MAP4 to label microtubules. We then recorded z-stacks of the entire oocyte volume during asymmetric spindle positioning using Zeiss' MultiTime Series macro (11 sections; spacing: 8 μm; time interval: 10 min). We corrected for drifts during image acquisition with the 'correct drift' function of the image analysis software Imaris (Bitplane) after segmenting the oocyte volume by applying a low threshold on the soluble pool of the fluorescent reporter. Afterwards we segmented the spindle by applying a higher threshold and tracked the spindle's centre of mass during spindle movement using Imaris. For averaging the spindle movements in different oocytes, we temporally aligned the different data sets to the time when the spindle slowed down due to arrival at the cortex. In oocytes, where the spindle did not reach the cortex, the data sets were aligned to time points corresponding to the end of asymmetric spindle positioning in controls. The distance of the spindle to the alignment position was calculated for each time point by processing the spindle coordinates in Excel and plotted over time. To calculate average spindle speeds, the spindle velocity in each oocyte was calculated by linear regression analysis of the displacement plots. Average, standard deviation, and statistical significance based on Student's t-test were calculated in Excel.

Automated quantification of the number and volume of vesicles

To label vesicles, oocytes were microinjected with mRNA encoding fluorescently labelled Rab11a or Spire2 and arrested in dbcAMP until the fluorescent reporter protein was expressed. Oocytes were then released into dbcAMP free medium. 3D data sets of vesicles were acquired using Zeiss' MultiTime Series. The number of vesicles was determined using the spot detection function in Imaris. The vesicle volume was reconstructed by using the region growing function during spot detection in Imaris. The number of vesicles in a defined oocyte volume and the vesicle volume were then exported into Excel. In Figure 5j, the number of vesicles was normalized to the average number of vesicles within the first three minutes of BFA or methanol addition. Average, standard deviation, and statistical significance based on Student's t-test were calculated in Excel.

Quantification of cytoplasmic mEGFP-Spire2 intensity upon BFA addition

The intensity of mEGFP-Spire2 in the cytoplasm upon BFA or methanol addition in Figure 5k and Supplementary Figure S8a was measured in ImageJ. Vesicles were excluded from the evaluated area by thresholding. For background subtraction, the intensity in an area outside the oocyte was measured. Measurements were repeated for all five z-sections and averaged. Intensities were normalized relative to the intensity in the first frames after BFA or methanol addition. Since imaging was started at slightly variable times after BFA addition, the data sets were aligned to the time when the increase in mEGFP-Spire2 intensity had reached half its maximum.

Statistics

Average (mean), s.d. and statistical significance based on Student's t –test (always two-tailed) were calculated in Excel. The sample size was chosen based on Student's t-test. All box plots show median (line), mean (small square), 1st, 99th (crosses), 5th, 95th (whiskers) and 25th and 75th percentile (boxes).

Supplementary Material

Refer to Web version on PubMed Central for supplementary material.

Acknowledgments

The authors thank the staff of the LMB's Animal Facility for expert technical assistance; and J. Ellenberg, M. Freeman, A.R. Hand, L.A. Jaffe, P. Lenart, S. Munro, B. Nichols and members of the Schuh lab for helpful discussions and comments on the manuscript. The research leading to these results has received financial support from the European Community's Seventh Framework Programme (FP7/2007-2013) under grant agreement no. 241548.

REFERENCES

1. Gardel ML, Schneider IC, Aratyn-Schaus Y, Waterman CM. Mechanical integration of actin and adhesion dynamics in cell migration. Annu. Rev. Cell Dev. Biol. 2010; 26:315–333. [PubMed: 19575647]
2. Michelot A, Drubin DG. Building distinct actin filament networks in a common cytoplasm. Curr. Biol. 2011; 21:R560–569. [PubMed: 21783039]
3. Field CM, Lénárt P. Bulk cytoplasmic actin and its functions in meiosis and mitosis. Curr. Biol. 2011; 21:R825–830. [PubMed: 21996509]
4. Fededa JP, Gerlich DW. Molecular control of animal cell cytokinesis. Nat. Cell Biol. 2012; 14:440–447. [PubMed: 22552143]
5. Pollard TD. Mechanics of cytokinesis in eukaryotes. Curr. Opin. Cell Biol. 2010; 22:50–56. [PubMed: 20031383]
6. Levayer R, Lecuit T. Biomechanical regulation of contractility: spatial control and dynamics. Trends Cell Biol. 2012; 22:61–81. [PubMed: 22119497]
7. Munro E, Nance J, Priess JR. Cortical flows powered by asymmetrical contraction transport PAR proteins to establish and maintain anterior-posterior polarity in the early C. elegans embryo. Dev. Cell. 2004; 7:413–424. [PubMed: 15363415]
8. Lecuit T, Lenne P-F, Munro E. Force generation, transmission, and integration during cell and tissue morphogenesis. Annu. Rev. Cell Dev. Biol. 2011; 27:157–184. [PubMed: 21740231]
9. Rauzi M, Lenne P-F, Lecuit T. Planar polarized actomyosin contractile flows control epithelial junction remodelling. Nature. 2010; 468:1110–1114. [PubMed: 21068726]
10. Tseng Y, Wirtz D. Dendritic branching and homogenization of actin networks mediated by arp2/3 complex. Phys. Rev. Lett. 2004; 93:258104. [PubMed: 15697951]
11. Bugyi B, Carlier M-F. Control of actin filament treadmilling in cell motility. Annu Rev Biophys. 2010; 39:449–470. [PubMed: 20192778]
12. Reymann A-C, et al. Actin network architecture can determine myosin motor activity. Science. 2012; 336:1310–1314. [PubMed: 22679097]
13. Azoury J, et al. Spindle positioning in mouse oocytes relies on a dynamic meshwork of actin filaments. Curr. Biol. 2008; 18:1514–1519. [PubMed: 18848445]
14. Pfender S, Kuznetsov V, Pleiser S, Kerkhoff E, Schuh M. Spire-type actin nucleators cooperate with Formin-2 to drive asymmetric oocyte division. Curr. Biol. 2011; 21:955–960. [PubMed: 21620703]
15. Quinlan ME, Heuser JE, Kerkhoff E, Mullins RD. Drosophila Spire is an actin nucleation factor. Nature. 2005; 433:382–388. [PubMed: 15674283]
16. Schuh M, Ellenberg J. A new model for asymmetric spindle positioning in mouse oocytes. Curr. Biol. 2008; 18:1986–1992. [PubMed: 19062278]
17. Schuh M. An actin-dependent mechanism for long-range vesicle transport. Nat. Cell Biol. 2011; 13:1431–1436. [PubMed: 21983562]
18. Stenmark H. Rab GTPases as coordinators of vesicle traffic. Nat. Rev. Mol. Cell Biol. 2009; 10:513–525. [PubMed: 19603039]
19. Hammer JA 3rd, Sellers JR. Walking to work: roles for class V myosins as cargo transporters. Nat. Rev. Mol. Cell Biol. 2012; 13:13–26. [PubMed: 22146746]
20. Ross JL, Ali MY, Warshaw DM. Cargo transport: molecular motors navigate a complex cytoskeleton. Curr. Opin. Cell Biol. 2008; 20:41–47. [PubMed: 18226515]

21. Leader B, et al. Formin-2, polyploidy, hypofertility and positioning of the meiotic spindle in mouse oocytes. Nat. Cell Biol. 2002; 4:921–928. [PubMed: 12447394]
22. Kerkhoff E, et al. The Spir actin organizers are involved in vesicle transport processes. Curr Biol. 2001; 11:1963–1968. doi:S0960-9822(01)00602-9 [pii]. [PubMed: 11747823]
23. Stoorvogel W, Oorschot V, Geuze HJ. A novel class of clathrin-coated vesicles budding from endosomes. The Journal of cell biology. 1996; 132:21–33. [PubMed: 8567724]
24. Futter CE, et al. In polarized MDCK cells basolateral vesicles arise from clathrin-gamma-adaptin-coated domains on endosomal tubules. The Journal of cell biology. 1998; 141:611–623. [PubMed: 9566963]
25. Wang E, Pennington JG, Goldenring JR, Hunziker W, Dunn KW. Brefeldin A rapidly disrupts plasma membrane polarity by blocking polar sorting in common endosomes of MDCK cells. J Cell Sci. 2001; 114:3309–3321. [PubMed: 11591819]
26. Pagano A, Crottet P, Prescianotto-Baschong C, Spiess M. In vitro formation of recycling vesicles from endosomes requires adaptor protein-1/clathrin and is regulated by rab4 and the connector rabaptin-5. Molecular biology of the cell. 2004; 15:4990–5000. doi:10.1091/mbc.E04-04-0355. [PubMed: 15331762]
27. Wang L, et al. Brefeldin A disrupts asymmetric spindle positioning in mouse oocytes. Developmental Biology. 2008; 313:155–166. [PubMed: 18053978]
28. Azoury J, Lee KW, Georget V, Hikal P, Verlhac MH. Symmetry breaking in mouse oocytes requires transient F-actin meshwork destabilization. Development. 2011; 138:2903–2908. doi: 10.1242/dev.060269. [PubMed: 21653611]
29. Vavylonis D, Wu J-Q, Hao S, O'Shaughnessy B, Pollard TD. Assembly mechanism of the contractile ring for cytokinesis by fission yeast. Science. 2008; 319:97–100. [PubMed: 18079366]
30. Woolner S, O'Brien LL, Wiese C, Bement WM. Myosin-10 and actin filaments are essential for mitotic spindle function. The Journal of cell biology. 2008; 182:77–88. doi:10.1083/jcb. 200804062. [PubMed: 18606852]
31. Dahlgaard K, Raposo AA, Niccoli T, St Johnston D. Capu and Spire assemble a cytoplasmic actin mesh that maintains microtubule organization in the Drosophila oocyte. Dev Cell. 2007; 13:539–553. [PubMed: 17925229]
32. Taunton J, et al. Actin-dependent propulsion of endosomes and lysosomes by recruitment of N-WASP. The Journal of cell biology. 2000; 148:519–530. [PubMed: 10662777]
33. Field CM, et al. Actin behavior in bulk cytoplasm is cell cycle regulated in early vertebrate embryos. J Cell Sci. 2011; 124:2086–2095. doi:10.1242/jcs.082263. [PubMed: 21610091]
34. Schuh M, Ellenberg J. Self-organization of MTOCs replaces centrosome function during acentrosomal spindle assembly in live mouse oocytes. Cell. 2007; 130:484–498. [PubMed: 17693257]
35. Shaner NC, et al. Improved monomeric red, orange and yellow fluorescent proteins derived from Discosoma sp. red fluorescent protein. Nat. Biotechnol. 2004; 22:1567–1572. [PubMed: 15558047]
36. Bucci C, et al. The small GTPase rab5 functions as a regulatory factor in the early endocytic pathway. Cell. 1992; 70:715–728. [PubMed: 1516130]
37. Hume AN, et al. Rab27a regulates the peripheral distribution of melanosomes in melanocytes. J. Cell Biol. 2001; 152:795–808. [PubMed: 11266470]
38. Liman ER, Tytgat J, Hess P. Subunit stoichiometry of a mammalian K+ channel determined by construction of multimeric cDNAs. Neuron. 1992; 9:861–871. [PubMed: 1419000]
39. Burkel BM, von Dassow G, Bement WM. Versatile fluorescent probes for actin filaments based on the actin-binding domain of utrophin. Cell Motil. Cytoskeleton. 2007; 64:822–832. [PubMed: 17685442]
40. Chinga G, Syverud K. Quantification of paper mass distributions within local picking areas. Nordic Pulp Paper Res. J. 2007; 22:441–446.

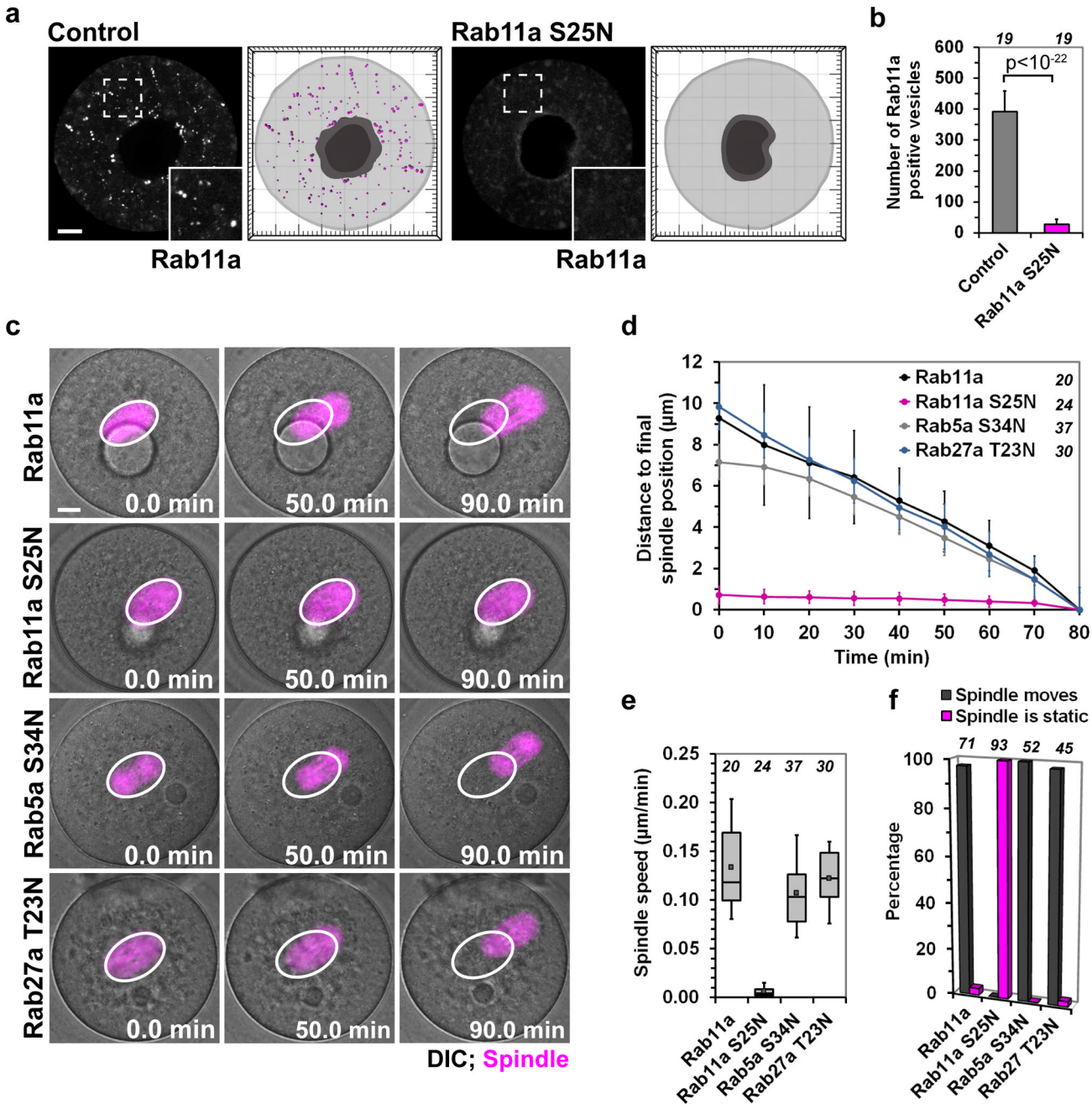

Figure 1. Asymmetric spindle positioning in oocytes requires Rab11a-positive vesicles

(a) mEGFP-Rab11a localization in control oocytes expressing mEGFP-Rab11a and in oocytes expressing mEGFP-Rab11a together with mCherry-Rab11a S25N (Rab11a S25N) (z-projection, 5 sections, every 0.66 μm). Boxed regions are magnified in inset. Scale bar, 10 μm. Isosurfaces of the oocyte (light grey), nucleus (dark grey) and vesicles (magenta) were reconstructed from oocytes shown left.

(b) The number of Rab11a-positive vesicles in control and dominant-negative Rab11a expressing oocytes is shown. Vesicles were identified and counted with the spot detection function of Imaris in an oocyte segment of 20×20×20 μm^3. The number of analysed oocytes

is specified in italics (aggregation over 3 independent experiments). Data are mean, with error bars displaying s.d.. *P* values were calculated with Student's t-test.
(c) Spindle movements in live oocytes expressing EGFP-MAP4 (magenta, microtubules, merged with differential interference contrast [DIC]). Oocytes express mCherry fused to Rab11a (Rab11a), dominant-negative Rab11a (Rab11a S25N), dominant-negative Rab5a (Rab5a S34N) or dominant-negative Rab27a (Rab27a T23N). White ovals mark initial spindle positions. Scale bar, 10 μm.
(d) The spindle was tracked in 3D data sets (11 sections, every 8 μm) of oocytes as shown in (c) and spindle movements were plotted. The number of analysed oocytes is specified in italics (aggregation over 3-4 independent experiments). Data are mean, with error bars displaying s.d..
(e) The spindle speeds were determined from the plots in (d). The box plot shows median (line), mean (small square), 25^{th}, 75^{th} (boxes), 5^{th} and 95^{th} percentile (whiskers) of spindle speeds. The number of analysed oocytes is specified in italics.
(f) The efficiency of asymmetric spindle positioning in oocytes as shown in (c) is plotted. The number of analysed oocytes is specified in italics, (aggregation over 4-9 independent experiments).

Europe PMC Funders Author Manuscripts

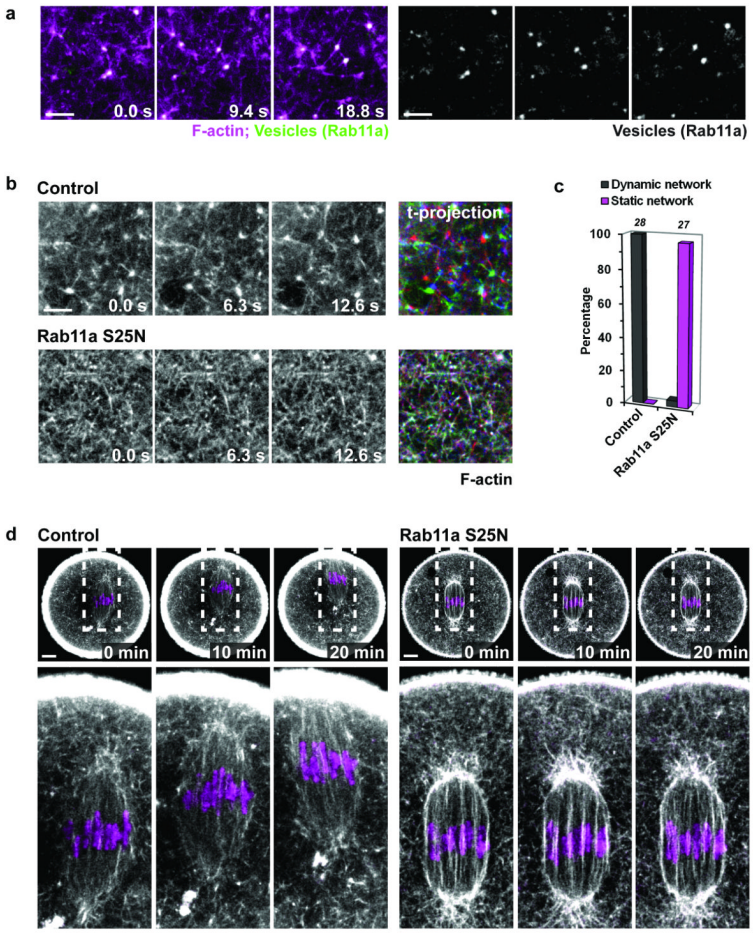

Figure 2. Rab11a-positive vesicles drive the actin network dynamics

(a) Oocyte expressing EGFP-UtrCH (F-actin) together with mCherry-Rab11a (Vesicles). A merge of the F-actin (magenta) and vesicle (green) localization is shown on the left, and the vesicle localization separately on the right. Representative example from 4 independent experiments (>40 oocytes total). Scale bar, 5 μm.

(b) F-actin dynamics in oocytes expressing EGFP-UtrCH (F-actin) together with mCherry-Rab11a (Control) or dominant-negative Rab11a (Rab11a S25N). Projections are time-coloured in RGB (green, blue and red with increasing time). Scale bar, 5 μm.

(c) The percentage of oocytes with a dynamic or static actin network is shown. An image correlation coefficient below 0.5 after 30 s was scored as dynamic and above 0.5 as static. The number of analysed oocytes is specified in italics (aggregation over 2 independent experiments).

(d) Oocytes expressing EGFP-UtrCH (F-actin; single section) together with mCherry-Rab11a (Control) or dominant-negative mCherry-Rab11a (Rab11a S25N). Chromosomes (magenta; z-projection: 3 sections every 1.2 μm) were labelled with Hoechst. Boxed region is magnified below. Representative examples from 3 independent experiments (30 oocytes total for each condition). Same oocytes as in Supplementary Video 4. Scale bar, 10 μm.

Europe PMC Funders Author Manuscripts

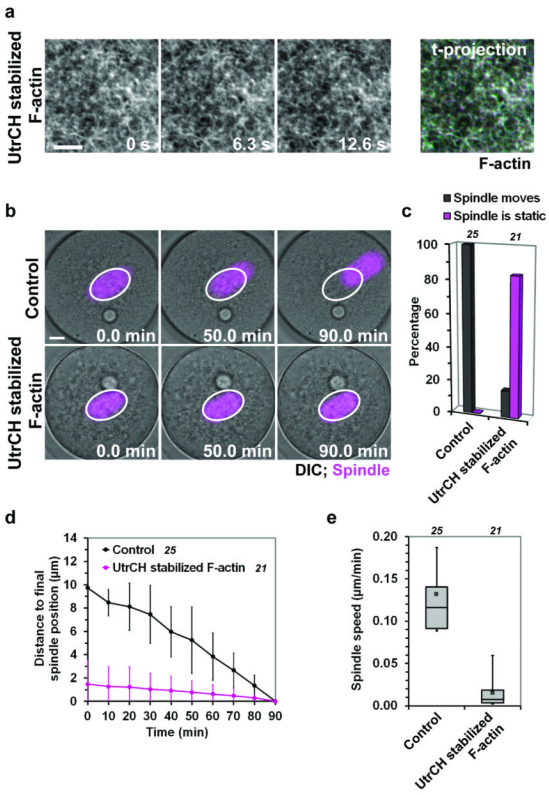

Figure 3. Blocking vesicle-actin-network dynamics prevents asymmetric spindle positioning

(a) Oocyte expressing very high amounts of EGFP-UtrCH (F-actin). Projection is time-coloured in RGB. Scale bar, 5 μm.

(b) Spindle movements (magenta, mCherry-MAP4; microtubules, merged with differential interference contrast [DIC]) in live control oocyte (Control) and oocyte expressing very high amounts of EGFP-UtrCH to stabilize F-actin (UtrCH stabilized F-actin). White ovals mark initial spindle positions. Scale bar, 10 μm.

(c) The efficiency of asymmetric spindle positioning in oocytes as shown in (b) is plotted. The number of analysed oocytes is specified in italics, (aggregation over 2 independent experiments).

(d) The spindle was tracked in oocytes in 3D data sets (11 sections, every 8 μm) as shown in (b) and spindle movements were plotted. The number of analysed oocytes is specified in italics (aggregation over 2 independent experiments). Data are mean, with error bars displaying s.d..

(e) The spindle speeds were determined from the plots in (d). Box plot as in Figure 1e. The number of analysed oocytes is specified in italics.

Europe PMC Funders Author Manuscripts

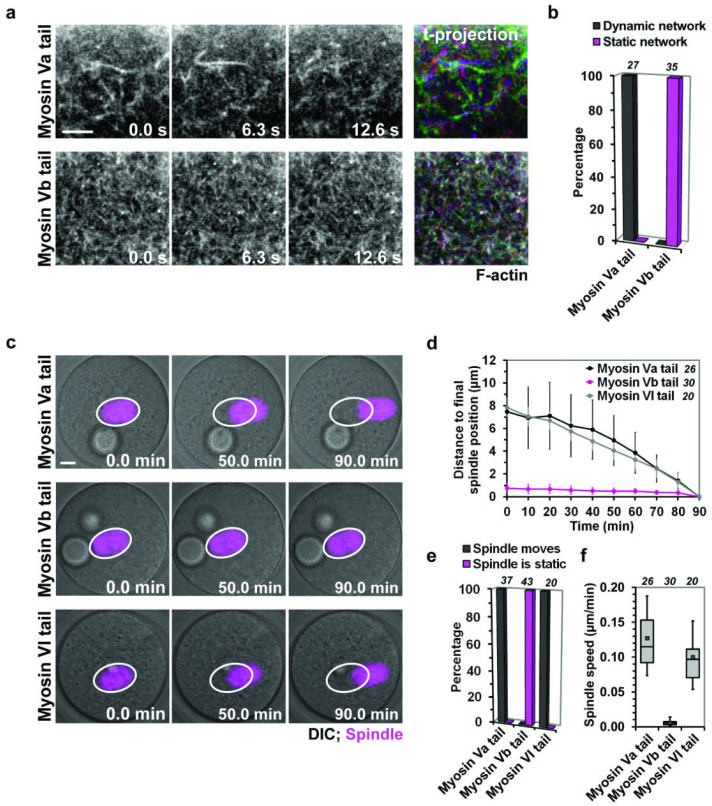

Figure 4. Myosin Vb mediates the actin network dynamics and asymmetric spindle positioning

(a) Oocytes expressing EGFP-UtrCH (F-actin) together with mCherry fusion proteins of dominant-negative myosin Va (Myosin Va tail) or dominant-negative myosin Vb (Myosin Vb tail; lower row). Projections are time-coloured in RGB. Scale bar, 5 µm.

(b) The percentage of oocytes with a dynamic or static actin network is shown. An image correlation coefficient below 0.5 after 30 s was scored as dynamic and above 0.5 as static. The number of analysed oocytes is specified in italics (aggregation over 2 independent experiments).

(c) Spindle movements in live oocytes expressing EGFP-MAP4 (magenta, microtubules, merged with differential interference contrast [DIC]). Oocytes express mCherry fused to dominant-negative myosin Va (Myosin Va tail), dominant-negative myosin Vb (Myosin Vb tail), or dominant-negative myosin VI (Myosin VI tail). White ovals mark initial spindle positions. Scale bar, 10 µm.

(d) The spindle was tracked in oocytes in 3D data sets (11 sections, every 8 µm) as shown in (c) and spindle movements were plotted. The number of analysed oocytes is specified in italics (aggregation over 2-3 independent experiments). Data are mean, with error bars displaying s.d..

(e) The efficiency of asymmetric spindle positioning in oocytes as shown in (c) is plotted. The number of analysed oocytes is specified in italics (aggregation over 2-4 independent experiments).

(f) The spindle speeds were determined from the plots in (d). Box plot as in Figure 1e. The number of analysed oocytes is specified in italics.

Europe PMC Funders Author Manuscripts

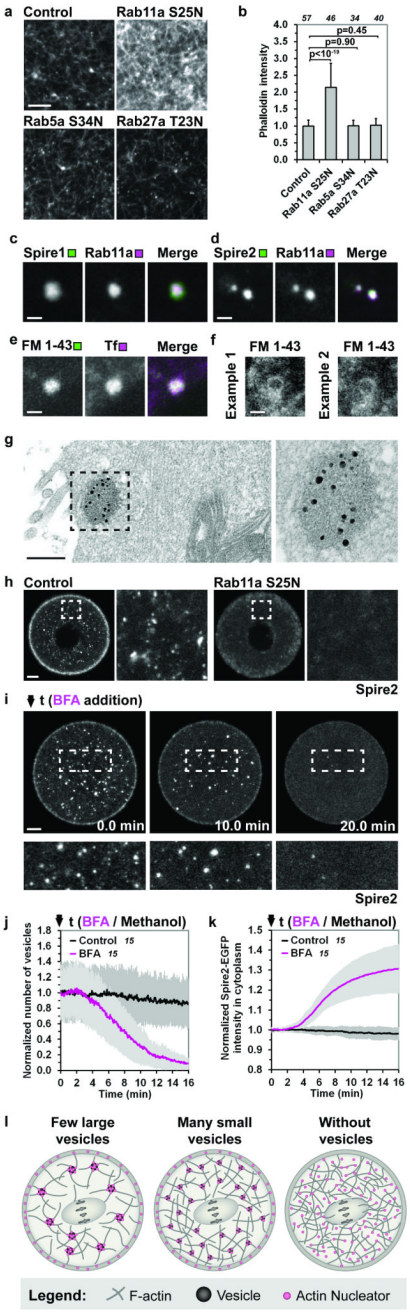

Figure 5. Rab11a-positive vesicles modulate the actin network density

(a) Oocytes expressing mCherry-Rab11a (Control), dominant-negative mCherry-Rab11a (Rab11a S25N), dominant-negative mCherry-Rab5a (Rab5a S34N) or dominant-negative mCherry-Rab27a (Rab27a T23N) were fixed and stained for F-actin. Scale bar, 5 μm.

(b) The mean intensity of F-actin in the cytoplasm (labelled by fluorescent phalloidin) was measured in oocytes as shown in (a). Data are mean, with error bars displaying s.d.. The number of analysed oocytes is specified in italics (aggregation over 3 independent experiments). *P* values were calculated with Student's t-test.

Europe PMC Funders Author Manuscripts

(c,d) Live oocytes expressing mEGFP-Spire1 and mCherry-Rab11a (c) or mEGFP-Spire2 and mCherry-Rab11a (d). Representative examples from 2 (c) or 6 (d) independent experiments (>15 oocytes total for each condition). Scale bar, 2 μm.
(e) Live oocyte labelled with FM 1-43 and Alexa Fluor 488-transferrin. Representative example from 2 independent experiments (>10 oocytes total). Scale bar, 2 μm.
(f) FM1-43 labelled membrane compartment in same oocyte as shown in (e), imaged with identical imaging conditions as in (e). Representative examples from 2 independent experiments (>10 oocytes total). Scale bar, 2 μm.
(g) mEGFP-Spire2 localization in anti-GFP immunogold labelled oocytes. Boxed regions are magnified next to overview. Representative example from 5 independent experiments (23 oocytes total). Two other examples are shown in Supplementary Fig. S7d. Scale bar, 200 nm.
(h) mEGFP-Spire2 localization in oocytes expressing mCherry-Rab11a (Control) or dominant-negative mCherry-Rab11a (Rab11a S25N) (z-projection, 5 sections, every 0.66 μm). Representative examples from 6 independent experiments (>70 oocytes total for each condition). Scale bar, 10 μm. Boxed region is magnified on the right.
(i) mEGFP-Spire2 localization in live oocytes upon addition of 10 μM BFA (z-projection, 5 sections, every 0.66 μm). Scale bar, 10 μm. Boxed region is magnified below. A corresponding control experiment with methanol addition is shown in Supplementary Fig. S8a.
(j, k) The number of Spire2-positive vesicles (j) and the intensity of mEGFP-Spire2 in the cytoplasm (k) upon addition of BFA or methanol (Control) was quantified in data sets as shown in (i) and Supplementary Fig. S8a. Vesicles were identified and counted with the spot detection function of Imaris in an oocyte segment of 20×20×20 μm^3 and normalized to the initial number of vesicles. Data are mean, with error bars displaying s.d.. The number of analysed oocytes is specified in italics (aggregation over 3 independent experiments).
(l) Schematic illustrating the localization of actin nucleators and changes in actin network density in oocytes with different numbers of Rab11a-positive vesicles

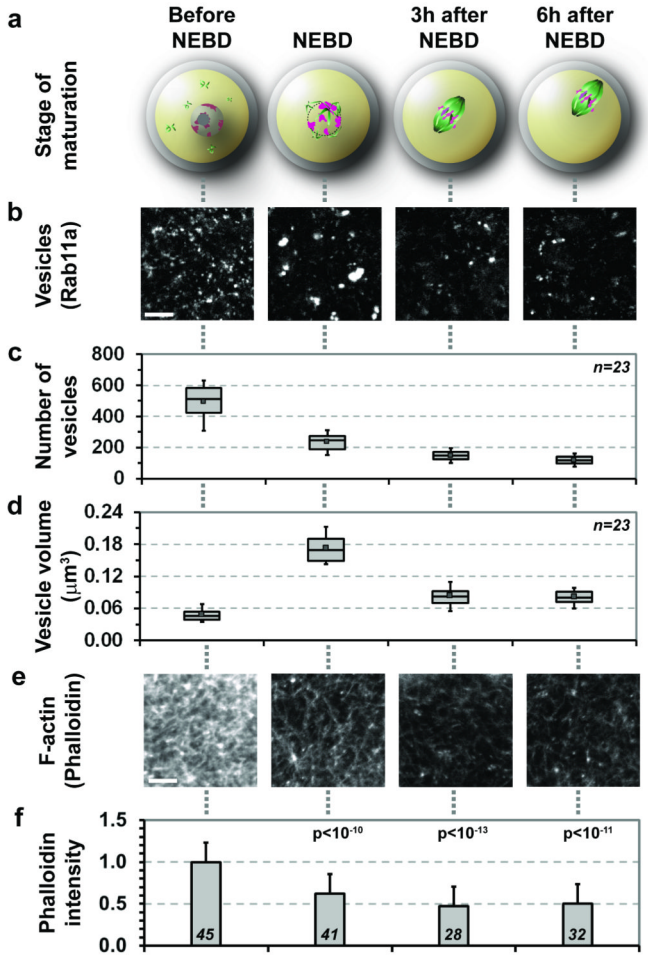

Figure 6. The actin network density and the number of vesicles correlate in different stages of oocyte maturation

(a) Scheme illustrating different stages of oocyte maturation. The images and data points below (b-f) correspond to these stages.

(b) Vesicles in different stages of maturation in oocytes expressing mEGFP-Spire2 (z-projection: 5 sections, every 0.66 μm).

(c) The number of vesicles was quantified in data sets as shown in (b). Vesicles were identified and counted with the spot detection function of Imaris in a volume of 20×20×20 μm^3. The number of analysed oocytes is specified in italics (aggregation over 2 independent experiments). Box plot as in Figure 1e.

(d) The vesicle volume was quantified in data sets as shown in (b). The vesicle volume was measured using the region growing function in Imaris in a volume of 20×20×20 μm^3. The number of analysed oocytes is specified in italics (aggregation over 2 independent experiments). Box plot as in Figure 1e.

(e) Oocytes were fixed at the different stages of oocyte maturation shown in (a) and stained for F-actin using fluorescent phalloidin. Scale bar, 5 μm.

(f) The mean intensity of the cytoplasmic phalloidin staining was measured in oocytes as shown in (e). Error bars display s.d.. *P* values relative to 'Before NEBD' stage were calculated with Student's t-test. The number of analysed oocytes is specified in italics (aggregation over 3 independent experiments).

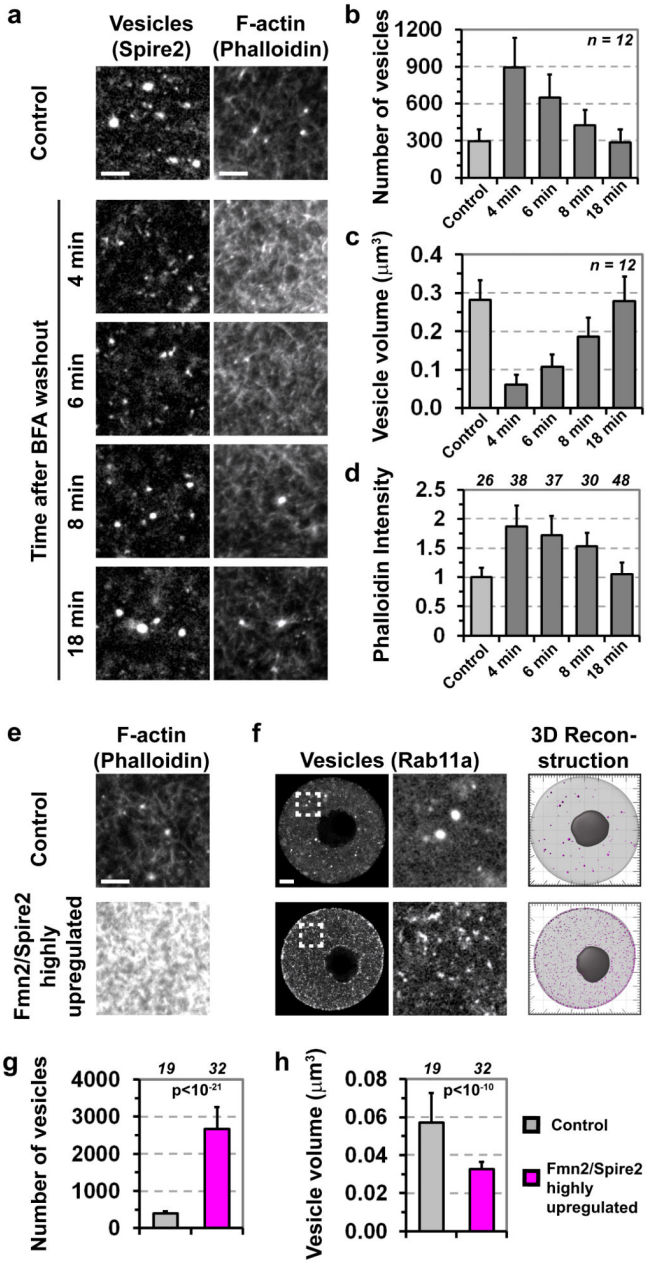

Figure 7. The actin network density is closely coupled to the number of vesicles

(a) Control oocytes and oocytes that were released from BFA at the indicated times were imaged live while expressing mEGFP-Spire2 (left row) or fixed and stained for F-actin (right row). Scale bar, 5 μm.

(b) The number of vesicles was quantified in data sets as shown in (a). The number of vesicles in a volume of 20×20×20 μm^3 is displayed. Data are mean, with error bars displaying s.d.. The number of analysed oocytes is specified in italics (aggregation over 2-3 independent experiments).

(c) The vesicle volume was quantified in data sets as shown in (a). Data are mean, with error bars displaying s.d.. The number of analysed oocytes is specified in italics (aggregation over 2-3 independent experiments).

(d) The mean intensity of F-actin in the cytoplasm (labelled by fluorescent phalloidin) was measured in oocytes as shown in (a). Error bars display s.d.. The number of analysed oocytes is specified in italics (aggregation over 3 independent experiments).
(e) Wildtype oocytes (Control) and oocytes highly overexpressing Fmn2-mCherry and mCherry-Spire2 (Fmn2 and Spire2 highly upregulated) were fixed and stained for F-actin. Representative examples from 2 independent experiments (>10 oocytes total for each condition). Scale bar, 5 μm.
(f) mEGFP-Rab11a in control oocytes and oocytes highly overexpressing Fmn2-mCherry and mCherry-Spire2 (Fmn2 and Spire2 highly upregulated). Boxed region is magnified on the right. Scale bar, 10 μm. In contrast to Fig. 1a, only a single section is shown. Isosurface reconstructions show oocyte (light grey), nucleus (dark grey) and vesicles (magenta) .
(g) The number of vesicles was quantified in data sets as shown in (f). The number of vesicles in a volume of 20×20×20 μm^3 is displayed. Data are mean, with error bars displaying s.d.. *P* value was calculated with Student's t-test. The number of analysed oocytes is specified in italics (aggregation over 2-3 independent experiments).
(h) The vesicle volume was quantified in data sets as shown in (f). Data are mean, with error bars displaying s.d.. *P* value was calculated with Student's t-test. The number of analysed oocytes is specified in italics (aggregation over 2-3 independent experiments).

Europe PMC Funders Author Manuscripts

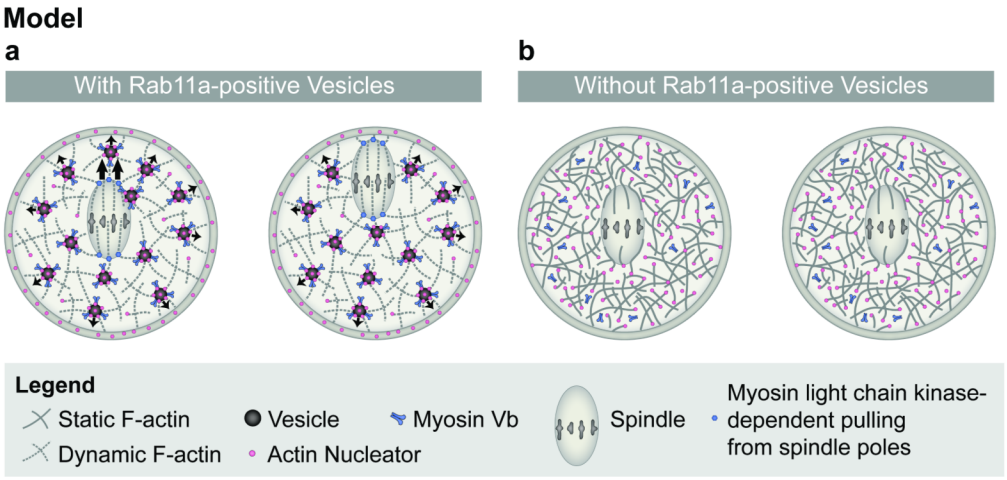

Figure 8. Model for how Rab11a-positive vesicles modulate the actin network for asymmetric spindle positioning

(a) In the presence of Rab11a-positive vesicles, the vesicles drive the dynamics of the actin network in a myosin Vb-dependent manner. The actin network density is low, because actin nucleators are clustered and sequestered at vesicles. The outward-directed dynamics of the vesicles and their associated actin filaments drive asymmetric spindle positioning.

(b) Without Rab11a-positive vesicles, the actin network is static. The actin network density is increased, because actin nucleators are released from vesicles. The static network prevents asymmetric spindle positioning.

Europe PMC Funders Author Manuscripts